COMMISSIONING OF THE INJECTOR SYSTEM FOR THE X-BAND ELECTRON LINEAR ACCELERATOR IN MELBOURNE

J. Valerian*, M. Volpi, P. Pushkarna, P. Giansiracusa[1], R. Rassool, S. L. Sheehy[2], V. Lu
University of Melbourne, Melbourne, Australia
R. Dowd, Y.-R. E. Tan, Australian Synchrotron - ANSTO, Melbourne, Australia
[1]also at Australian Synchrotron - ANSTO, Melbourne, Australia
[2]also at ANSTO, Sydney, Australia

Abstract

The University of Melbourne's X-band Laboratory for Accelerators and Beams (X-LAB) is developing a compact electron linear accelerator. The injector system will consist of a 100-keV DC photogun, a pulsed UV laser, an S-band (2.9985 GHz) RF buncher, and magnetic elements for beam transport. This paper reports on the commissioning of the injector system. We present the characterisation of the test laser and buncher, as well as initial electron beam measurements with Faraday cup. Particle tracking simulations using General Particle Tracer (GPT) code were used to obtain approximate optimal solenoid currents. We also report on the conditioning of the photogun, including photocathode inspection, vacuum performance, dark current, and stray radiation.

INTRODUCTION

The University of Melbourne's X-band Laboratory for Accelerators and Beams (X-LAB) hosts the Mel-BOX, which is one half of XBox-3, a high-power RF test stand previously at CERN built to evaluate X-band (11.994 GHz) accelerators for the Compact Linear Collider (CLIC) collaboration [1, 2]. It was relocated and reassembled in Melbourne and is now fully operational [3]. Following reassembly, high-power conditioning has progressed well [4], and several studies on accelerator structure diagnostics have been carried out [5, 6]. In parallel, X-LAB has been developing an injector that may be used in conjunction with such high-power high-gradient X-band technology. In this paper, we present its current progress.

The injection system uses a 100 kV DC photogun where a laser generates the initial electrons which are then accelerated to 100 keV. The beam is then collimated and focused using solenoids before entering an S-band (2.9985 GHz) RF buncher. Upstream of the buncher, steering coils provide beam control, while correction coils compensate for the Earth's magnetic field. During commissioning, either a Faraday cup or the sample chamber is installed directly downstream of the buncher to characterise the photogun output as shown in Fig. 1. A nanosecond test laser is used in place of a picosecond laser, and the buncher is turned off. The commissioning setup is shown schematically in Fig. 2.

First, we discuss the photogun conditioning and issues encountered. The test laser characterisation is then presented,

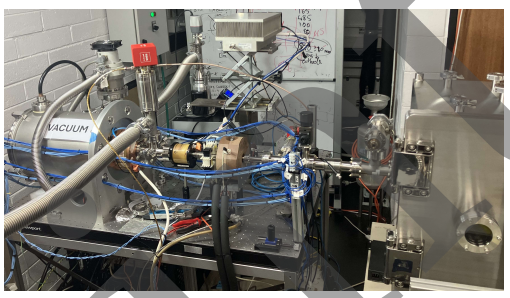

Figure 1: The injector status after reassembly. The laser enclosure is not shown.

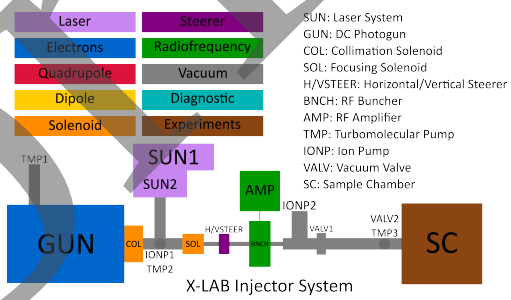

Figure 2: Schematic of the injector system during commissioning. Correction coils are omitted for clarity.

followed by General Particle Tracer (GPT) simulations to determine approximate optimal solenoid currents. Preliminary beam measurements are then reported, along with vector network analyser (VNA) measurements of the buncher S-parameters.

CONDITIONING

The photogun was conditioned to minimise dark current and suppress electric breakdown by first pumping the system down to high vacuum over approximately one week using turbomolecular pumps and ion pumps, followed by high-voltage training to 105 kV using the manufacturer's conditioning algorithm. A non-evaporable getter was occasionally activated to improve vacuum quality. Ideally, the pressure inside the photogun should be stable below 10^{-6} mbar, but we could only reach a few 10^{-6} mbar.

During high-voltage training, a faint blue spot was observed on the phosphor screen (Blue RE 800 Speed) in the sample chamber (Fig. 3). As the laser was disabled, this was attributed to dark current, estimated to be in the nanoampere range, while a few microamperes were measured at the pho-

* joel.valerian@student.unimelb.edu.au

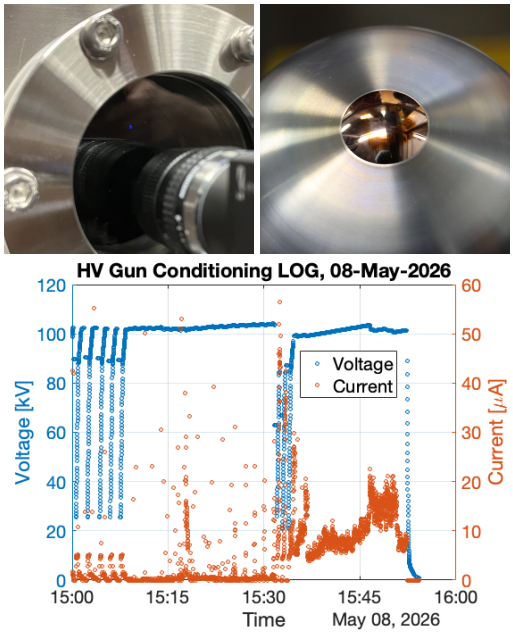

Figure 3: (Upper Left) Dark current observed on the phosphor screen. (Upper Right) Photocathode surface showing a faint contamination ring. (Bottom) Voltage and dark current measurement during high-voltage training where dark current become high after a particular breakdown.

tocathode. Over time, elevated stray radiation levels were also detected at the rear of the photogun, so we disassemble the photogun and replaced the photocathode with a spare.

Dark rings were observed on the photocathode surface (Fig. 3), likely caused by degradation during several years of storage, so we replaced it with a spare photocathode. A localised dark spot on the photogun insulation was also identified and removed by gentle polishing. The dark current issues were likely exacerbated by suboptimal vacuum conditions near the photocathode ($\sim 10^{-5}$ mbar) during conditioning, including persistent vacuum spikes after reaching the target voltage. During reassembly, a small leak was identified in the six-way cross directly downstream of the photogun and subsequently replaced. Reconditioning efforts were successful up to 100 kV, when a breakdown occured, after which the dark current and stray radiation became consistently high again, but this time with much more stable vacuum. This issue remains under investigation.

LASER

The photocathode is fabricated from high-purity oxygen-free copper, requiring UV photons (267 nm) for photoemission. The test laser is a passive Q-switched laser (MPL-F-266) that generates 266 nm output through successive frequency doubling of a 1064 nm fundamental, producing a coaxial three-wavelength output. The laser head is driven by a power supply unit with an external clock supplied by an arbitrary waveform generator (Agilent 33210A) operating at 2 kHz. A digital pulse generator (Stanford DG535) modulates the external clock pulse width to trigger the laser. Both

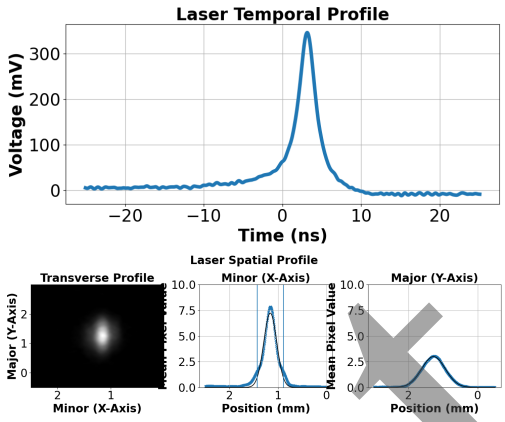

Figure 4: (Top) Temporal profile measured with the SiPM biased at 27 V and current-limited to 5 mA. (Bottom) Transverse profile measured at 600 mm from output window.

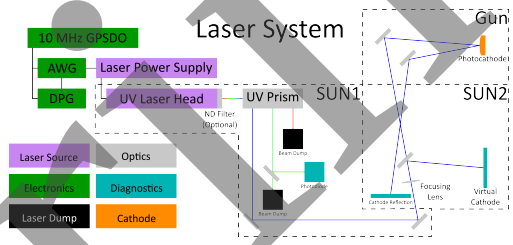

Figure 5: Laser system schematic showing trigger electronics and optical layout. AWG: Arbitrary Waveform Generator. DPG: Digital Pulse Generator.

instruments are synchronised to a 10 MHz GPS-disciplined oscillator (GPSDO). A neutral-density (ND) filter can be attached at the output for alignment, while a prism separates the three wavelength components. The IR and visible components are dumped, but the visible component is first sampled for temporal profile measurements using a silicon photomultiplier (onsemi C-series). The measured pulse profile is shown in Fig. 4. All three components are assumed to have equivalent pulse widths.

The UV component is guided toward the photogun using two kinematic mirrors and directed onto the photocathode via a mirror mounted within the six-way cross. A sampler is used to generate a virtual photocathode image on a UV card (Pyranine). A second internal mirror captures the reflected laser from the photocathode and directs it out into a second UV card for diagnostics. Both UV cards are imaged using a CCD camera (PGR Flea2). A schematic of the laser system is shown in Fig. 5. The measured and estimated laser parameters are summarised in Table 1. The jitter is defined as the standard deviation of the delay between the laser and trigger, while pulse energy is estimated from electron beam measurements.

SOLENOIDS

GPT simulations were used to model electron transport through the injector for varying collimation and focusing solenoid currents. Space-charge effects were assumed to be negligible at the current charge density and were therefore

Table 1: Characteristics of the Test Laser

Parameter	Value
Repetition Rate	2000 Hz
Pulse Width (FWTM)	4.75 ± 0.12 ns
Delay ± Jitter	125 ± 2.35 µs
Major Axis Width (FWHM)	0.80 mm
Minor Axis Width (FWHM)	0.32 mm
Pulse Energy	6.53 µJ ± 0.82%

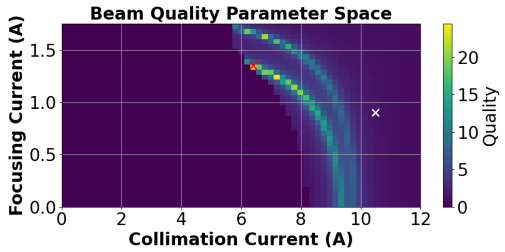

Figure 6: Heatmap showing the beam quality as a function of solenoid current. The red cross marks the maximum quality point, while the white cross marks the experimental value.

disabled to reduce simulation time. A quality index was defined as the sum of the inverse of the radial width and divergence at 1.075 m from the photocathode, multiplied by a transmission mask requiring 100% particle transport. The resulting heatmap is shown in Fig. 6, with optimal currents of approximately 6.4 A for the collimation solenoid and 1.35 A for the focusing solenoid. Experimentally, successful transport to the Faraday cup was achieved at 10.5 A and 0.9 A. The Earth's magnetic field and correction coils were not included in the simulation, which may account for the discrepancy. More comprehensive and realistic simulations will be performed in future work.

BEAM MEASUREMENTS

The beam charge was measured using a Faraday cup (RadiaBeam) terminated into 50 Ω and connected to a 4 GHz oscilloscope (Agilent Infiniium 54854A), as shown in Fig. 7. Integration of the measured pulse yielded approximately 700 mV·ns, corresponding to an average pulse charge of 14 pC. Assuming the manufacturer-specified quantum efficiency of 1×10^{-5}, the pulse energy is estimated to be 6.53 µJ. This corresponds to kilowatt-level peak power, but milliwatt-level average power. Attempts to observe the beam using a phosphor screen were unsuccessful due to insufficient intensity and excessive dark current.

BUNCHER

The buncher S-parameters were measured using a VNA (Anritsu MS46322B) with a typical output power of −3 dBm. A chiller was used to stabilise and control the buncher temperature. The relationship between resonant frequency and temperature, together with the measured S_{11} parameter at 45 °C, is shown in Fig. 8. The measured resonance shift is

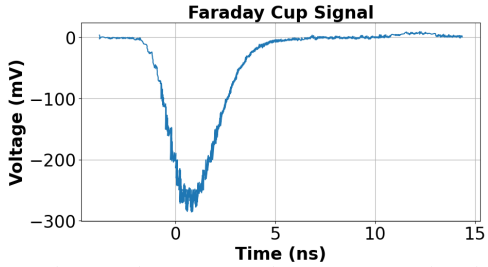

Figure 7: The Faraday cup signal is proportional to the beam current.

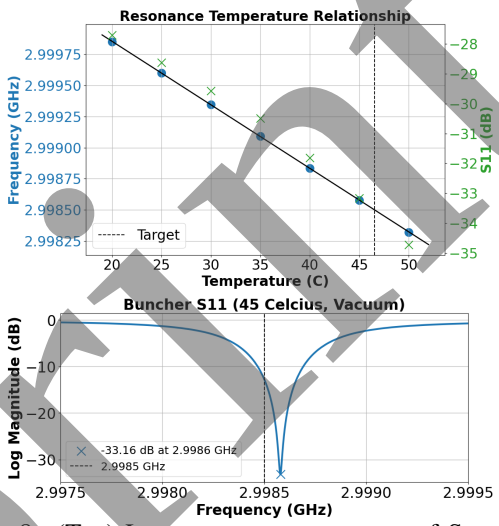

Figure 8: (Top) Low power measurement of S_{11} of the buncher over a range of temperatures. (Bottom) S_{11} response at 45 °C under vacuum.

51 kHz/°C. Under low-power operation, the buncher must be maintained at 46.6 °C to resonate at the target frequency.

Additional correction is required due to self-heating during high-power operation. The buncher is rated for 50 W average power (47 dBm) and 1000 W peak power (60 dBm). At maximum power, the required operating temperature shifts to 44.2 °C, corresponding to a temperature offset of −0.047 °C/dBm. Our amplifier is capable of 100 W (50 dBm). For operation with a 0.5 ms pulse width and 2.5 ms period (20% duty cycle), the average power is 20 W (43 dBm). This corresponds to a temperature correction of 2.2 °C, resulting in a final operating setpoint of 44.4 °C.

CONCLUSION

We successfully characterised the test laser and buncher, as well as demonstrated beam transport through the injector. Several issues contributing to elevated dark current and stray radiation were identified and investigated. Reconditioning efforts are still ongoing before moving on to the next phase of the project.

ACKNOWLEDGEMENTS

This paper is supported by Melbourne Research Scholarship and AINSE Travel Grant. We would like to thank Jim Franssen for the valuable help.

REFERENCES

[1] N. Catalán Lasheras *et al.*, "Commissioning of XBox-3: a very high capacity X-band test stand", in *Proc. LINAC 2016*, East Lansing, MI, USA, pp. 568–571, 2016. doi:10.18429/JACOW-LINAC2016-TUPLR047

[2] CLIC Collaboration, "CLIC readiness report", *Eur. Phys. J. Spec. Top*, vol. 234, pp. 6473–6652, 2026. doi:10.1140/epjs/s11734-025-02016-w

[3] M. Volpi *et al.*, "Commissioning of X-LAB: a very high-capacity X-band rf test stand facility at the University of Melbourne", in *Proc. IPAC'23*, Venice, Italy, pp. 3912–3915, 2023. doi:10.18429/JACoW-IPAC2023-THOGA1

[4] M. Volpi *et al.*, "High-power, high-repetition-rate X-band power source at X-LAB, the X-band laboratory for accelerators and beams at the University of Melbourne", in *Proc. IPAC'25*, Taipei, Taiwan, pp. 1896–1899, 2025. doi:10.18429/JACoW-IPAC2025-WEPB067

[5] P. Giansiracusa *et al.*, "Measurements of dark current and breakdown processes using Faraday cups and fast digitisers at the Xband Laboratory for Accelerators and Beams (XLAB)", in *Proc. IBIC'25*, Liverpool, UK, pp. 264–267, 2025. doi:10.18429/JACoW-IBIC2025-MOPMO35

[6] P. Pushkarna *et al.*, "Searches for RF breakdown precursors using Cherenkov light in optical fibers", in *Proc. IPAC'25*, Taipei, Taiwan, pp. 65–68, 2025. doi:10.18429/JACoW-IPAC2025-MOCN3